Monthly Notices
of the
ROYAL ASTRONOMICAL SOCIETY

MNRAS **465,** 3803–3816 (2017)
Advance Access publication 2016 September 26

doi:10.1093/mnras/stw2442

Illuminating gas inflows/outflows in the MUSE deepest fields: Lyα nebulae around forming galaxies at $z \simeq 3.3$

E. Vanzella,[1]★ I. Balestra,[2,3]★ M. Gronke,[4] W. Karman,[5] G. B. Caminha,[6] M. Dijkstra,[4] P. Rosati,[6] S. De Barros,[1,7] K. Caputi,[5] C. Grillo,[8,9] P. Tozzi,[10] M. Meneghetti,[1] A. Mercurio[11] and R. Gilli[1]

[1]*INAF – Osservatorio Astronomico di Bologna, via Ranzani 1, I-40127 Bologna, Italy*
[2]*University Observatory Munich, Scheinerstrasse 1, D-81679 Munich, Germany*
[3]*INAF – Osservatorio Astronomico di Trieste, via G. B. Tiepolo 11, I-34143 Trieste, Italy*
[4]*Institute of Theoretical Astrophysics, University of Oslo, Postboks 1029 Blindern, NO-0315 Oslo, Norway*
[5]*Kapteyn Astronomical Institute, University of Groningen, Postbus 800, NL-9700 AV Groningen, the Netherlands*
[6]*Dipartimento di Fisica e Scienze della Terra, Università di Ferrara, via Saragat 1, I-44122 Ferrara, Italy*
[7]*Observatoire de Genève, Université de Genève, 51 Ch. des Maillettes, CH-1290 Versoix, Switzerland*
[8]*Dark Cosmology Centre, Niels Bohr Institute, University of Copenhagen, Juliane Maries Vej 30, DK-2100 Copenhagen, Denmark*
[9]*Dipartimento di Fisica, Università degli Studi di Milano, via Celoria 16, I-20133 Milano, Italy*
[10]*INAF – Osservatorio Astrofisico di Arcetri, Largo E. Fermi, I-50125 Firenze, Italy*
[11]*INAF – Osservatorio Astronomico di Capodimonte, Via Moiariello 16, I-80131 Napoli, Italy*

Accepted 2016 September 23. Received 2016 September 21; in original form 2016 July 11; Editorial Decision 2016 September 22

ABSTRACT

We report the identification of extended Lyα nebulae at $z \simeq 3.3$ in the *Hubble Ultra Deep Field* (*HUDF*, $\simeq$40 kpc $\times$ 80 kpc) and behind the Hubble Frontier Field galaxy cluster MACSJ0416 ($\simeq$40 kpc), spatially associated with groups of star-forming galaxies. VLT/MUSE integral field spectroscopy reveals a complex structure with a spatially varying double-peaked Lyα emission. Overall, the spectral profiles of the two Lyα nebulae are remarkably similar, both showing a prominent blue emission, more intense and slightly broader than the red peak. From the first nebula, located in the *HUDF*, no X-ray emission has been detected, disfavouring the possible presence of active galactic nuclei. Spectroscopic redshifts have been derived for 11 galaxies within 2 arcsec from the nebula and spanning the redshift range $1.037 < z < 5.97$. The second nebula, behind MACSJ0416, shows three aligned star-forming galaxies plausibly associated with the emitting gas. In both systems, the associated galaxies reveal possible intense rest-frame-optical nebular emissions lines [O III] $\lambda\lambda$4959, 5007+Hβ with equivalent widths as high as 1500 Å rest frame and star formation rates ranging from a few to tens of solar masses per year. A possible scenario is that of a group of young, star-forming galaxies emitting ionizing radiation that induces Lyα fluorescence, therefore revealing the kinematics of the surrounding gas. Also Lyα powered by star formation and/or cooling radiation may resemble the double-peaked spectral properties and the morphology observed here. If the intense blue emission is associated with inflowing gas, then we may be witnessing an early phase of galaxy or a proto-cluster (or group) formation.

Key words: gravitational lensing: strong – radiative transfer – galaxies: distances and redshifts – galaxies: evolution – galaxies: starburst.

1 INTRODUCTION

Exchanges of gas between galaxies and the ambient intergalactic medium play an important role in the formation and evolution of galaxies. Circumgalactic gas at high redshift ($z > 3$) has been observed through absorption line studies using background sources close to foreground galaxies (e.g. Lanzetta et al. 1995; Møller & Warren 1998; Fynbo, Møller & Warren 1999; Chen et al. 2001; Adelberger et al. 2003; Fynbo et al. 2003; Steidel et al. 2010; Giavalisco et al. 2011; Turner et al. 2014). The presence of a significant amount of circumgalactic gas has also been revealed

★ E-mail: eros.vanzella@oabo.inaf.it (EV); italobale@gmail.com (IB)

through the detection of extended Lyα emission at several tens of kpc scales around single galaxies ($L_\alpha \simeq 10^{42}$ erg s^{-1}; e.g. Møller & Warren 1998; Steidel et al. 2010; Caminha et al. 2015; Patrício et al. 2016; Wisotzki et al. 2016) and up to hundreds of kpc scale around Quasi Stellar Objects (QSOs) and/or high-redshift radio galaxies ($L_\alpha \simeq 10^{44}$ erg s^{-1}; e.g. Cantalupo et al. 2014; Swinbank et al. 2015; Borisova et al. 2016).

While the origin of the extended Lyα emission is still debated, it is clear that the circumgalactic gas must be at least partly neutral. Extended Lyα emission is therefore a viable tool to investigate the presence, status and dynamics of the surrounding hydrogen gas, from single galaxies or galaxy groups. Various processes can be investigated, e.g. (1) the search for outflowing/inflowing material provides insights into feeding mechanism for galaxy formation and regulation on galactic baryonic/metal budgets and connection with the IGM, and (2) indirect signature of escaping ionizing radiation that illuminates inflowing/outflowing neutral hydrogen gas shaping the Lyα emission profile. The latter is connected with ionization capabilities of sources on their local environment (Rauch et al. 2011; Rauch, Becker & Haehnelt 2016).

The extent of Lyα nebula is found to be strongly related to the luminosity of a central source, with the largest nebulae extending to hundreds of kpc around luminous active galactic nucleus (e.g. Cantalupo et al. 2014; Hennawi et al. 2015; Swinbank et al. 2015; Borisova et al. 2016). The shape of these nebulae is often found to be symmetrical or filamentary around a central source (e.g. Hayes, Scarlata & Siana 2011; Patrício et al. 2016; Wisotzki et al. 2016), where more luminous sources show more circular morphologies. The central source is in agreement with proposed mechanisms responsible for extended emission, however, there are nebulae where no central source is detected (Prescott et al. 2012).

The diverse origin of Lyman-alpha blobs (LABs) can also be seen in the dynamics of Lyα nebulae. Most of the studied LABs have a chaotic distribution of Lyα emission (e.g. Christensen et al. 2004; Prescott et al. 2012; Francis et al. 2013; Caminha et al. 2015; Patrício et al. 2016) that is in agreement with Lyα scattering or an ionizing central source as the origin of the extended emission. The discovery of rotating LABs (e.g. Martin et al. 2015; Prescott, Martin & Dey 2015) indicates that also cold accretion flows can be responsible for extended Lyα emission.

In this work, we report on two very similar systems at approximately the same redshift ($z = 3.3$) discovered in two different fields: one recently observed with long-list spectroscopy by Rauch et al. (2011, 2016) in the *Hubble Ultra Deep Field* (*HUDF*, hereafter), and the second discovered as a multiply imaged system in the Hubble Frontier Fields cluster MACSJ0416. Both these systems have been observed with VLT/MUSE integral field spectroscopy, which revealed extended Lyα emission coincident with a group of star-forming galaxies. We present a study of morphology and spectral profile of these systems, possibly tracing outflowing and inflowing gas.

In the following discussion, we assume a flat cosmology with $\Omega_m = 0.3$, $\Omega_\Lambda = 0.7$ and $H_0 = 70$ km s^{-1} Mpc^{-1}, corresponding to 7.6 kpc proper for 1 arcsec separation at $z = 3.3$.

2 MUSE INTEGRAL FIELD SPECTROSCOPY

2.1 *HUDF* and Hubble Frontier Fields MACS J0416

The MUSE instrument mounted on the VLT (Bacon et al. 2012) is an efficient integral feld spectrograph highly suitable to blindly look for extended line emission. Its relatively large field of view (1 arcmin^2), spectral range (4750–9350 Å), relatively high spatial (0.2 arcsec) and spectral ($R \sim 3000$) resolution, and stability allowed us to discover extended Lyα emission, down to faint flux levels.

MUSE observations (Prog. ID 094.A-0289, P.I. Bacon) of the *HUDF* (Beckwith et al. 2006) were obtained between 2014 October and December. Data have been reduced using the standard ESO pipeline version 1.2.1. The raw calibration and science exposures of each single night have been processed, and combined into the final data cube (see Caminha et al. 2016 for a detailed description of the reduction process). We remind here that the wavelength calibration has been performed by fitting $\simeq$70 lines obtained from arc lamps of Ne, Xe and HgCd in each of the 24 slices of the instrument. The *rms* of the fit is $\sim$0.03 Å and the mean spectral resolution is $R = 3000 \pm 150$. The pipeline also produces spectra of the sky emission lines that we have used to further check the stability of the wavelength solution.

The seeing conditions were good, with an average of $\simeq$0.8 arcsec, and 81 per cent of the raw frames with seeing <1 arcsec based on the DIMM monitor at Paranal (the lack of bright stars in the pointing did not allow us to directly measure the seeing on MUSE data). Moreover, a visual inspection of all exposures (50 with DIT = 1500 s) from the stacked data cubes did not show evidence of significant variations in observational conditions. We obtain a reduced data cube centred at RA = 03h32m38s, DEC = $-27°46'44''$ of 19.5 h total integration time. We identified a spatially extended Lyα emission $\simeq$8 arcsec $\times$ 4 arcsec wide ($\simeq$80 $\times$ 40 proper kpc) at $z = 3.32$ in the *HUDF* centred at coordinates RA = 03h32m39.0s, DEC = $-27°46'17.0''$. The spectral line profile shows two main peaks, named 'red' and 'blue', hereafter, separated by a trough at $z \simeq 3.322$.

We also analysed MUSE data obtained on the North-Eastern portion of the Hubble Frontier Fields cluster MACS J0416 (Koekemoer et al. 2014; Lotz et al. 2014).[1] Data have been taken as part of the GTO programme 094.A-0115 (P.I. Richard).

Observations were obtained in 2014 November, for a total of 2 h divided in four exposures. Data have been reduced as described above (and we defer the reader to Caminha et al. 2016 for details) and produced a data cube of 2.0 h total integration time, centred at RA = 04h16m09.95s, DEC = $-24°04'01.9''$ with position angle 45°. Also in this field, we identified a strongly lensed Lyα nebula at $z = 3.33$ with a size of $\simeq$40 kpc proper with a spectral shape remarkably similar to the one discovered in the *HUDF*. Two multiple images of the lensed nebula have been identified at coordinates RA = 04h16m10.8s, DEC = $-24°04'20''.5$ and RA = 04h16m09.6s, DEC = $-24°04'00''.0$.

In the following, we focus on the details of these two systems. The basic properties are reported in Table 1.

3 LYα EMITTING NEBULA IN THE *HUDF*

3.1 Previous long-slit spectroscopy

A portion of the system studied in this work was observed with extremely deep, blind long-slit spectroscopy (Rauch et al. 2011) and, recently, with additional long-slit observations (Rauch et al. 2016). Rauch et al. (2016) reported a complex structure, i.e. diffuse, fan-like, blue-shifted Lyα emission and a DLA system in front of galaxy no. 10 (adopting our nomenclature, see panel C of Fig. 1, and discussion below). Various scenarios have been discussed, in

[1] http://www.stsci.edu/hst/campaigns/frontier-fields/

Table 1. List of parameters.

Lyα nebula – *HUDF*	
Right ascension (J2000):	03h32m39.0s
Declination (J2000):	$-27°46'17''.0$
Redshift (blue, red):	3.3172, 3.3266 (±0.0006)
L(Lyα) blue (erg s^{-1}):	$(5.5 \pm 0.1) \times 10^{42}$ erg s^{-1}
L(Lyα) red (erg s^{-1}):	$(4.0 \pm 0.1) \times 10^{42}$ erg s^{-1}
Possible galaxy counterparts	
no. 2-16373 (SFR; Mass)	4 M$_\odot$ yr^{-1}; 2.9×10^7 M$_\odot$
no. 3-16376 (SFR; Mass)	46 M$_\odot$ yr^{-1}; 1.2×10^9 M$_\odot$
no. 4-16148 (SFR; Mass)	0.1 M$_\odot$ yr^{-1}; 5.5×10^8 M$_\odot$
no. 6-16330 (SFR; Mass)	2 M$_\odot$ yr^{-1}; 3.2×10^7 M$_\odot$
no. 10-16506 (SFR; Mass)	100 M$_\odot$ yr^{-1}; 9.0×10^8 M$_\odot$
Lyα nebula – MACSJ0416	
Right ascension (J2000)[A]:	04h16m10.9s
Declination (J2000)[A]:	$-24°04'20''.7$
Right ascension (J2000)[B]:	04h16m09.6s
Declination (J2000)[B]:	$-24°03'59''.7$
Redshift (blue, red):	3.2840, 3.2928 (±0.0006)
L(Lyα) blue (erg s^{-1}):	$(4.4 \pm 0.1) \times 10^{42}$ erg s^{-1}
L(Lyα) red (erg s^{-1}):	$(3.7 \pm 0.1) \times 10^{42}$ erg s^{-1}
galaxy counterparts	adopting $\mu = 2$
no. 1439 (SFR; Mass)	0.7 M$_\odot$ yr^{-1}; 2.2×10^8 M$_\odot$
no. 1443 (SFR; Mass)	0.6 M$_\odot$ yr^{-1}; 1.5×10^9 M$_\odot$
no. 1485 (SFR; Mass)	1.7 M$_\odot$ yr^{-1}; 0.7×10^{10} M$_\odot$

particular the Lyα emission can be explained if the gas is inflowing along a filament behind the galaxy no. 10 and emits fluorescent Lyα photons induced by the ionizing flux escaping from the galaxy.

Long-slit spectroscopy, however, probes only a small volume and offers a marginal/limited view of the whole system. Our study benefits from a number of other key improvements over previous works: (i) the large field of view and spectral resolution of the MUSE instrument is essential for capturing many galaxies simultaneously in a single ultra-deep pointing, (ii) deep *HST* imaging observations cover the full MUSE field of view, (iii) homogeneous sub-arcsec spatial resolution for all objects is available. In the following, we describe the system as observed with MUSE.

3.2 Lyα nebula properties

Using the MUSE data cube we constructed 'pseudo-narrowband' (NB) images of the extended emission, centred on the position and wavelength of the corresponding Lyα line.

Before extracting the NB images, we performed an additional preprocessing as described in the following. At the low flux levels of interest in this study, source crowding becomes a serious issue for many objects. Several close neighbours within a few arcsec in projection are visible in the *HST* data. Since these neighbours are typically foreground sources, they contaminate the NB signal only with their continuum emission. A conventional method to remove the contaminating continuum is to subtract a suitably scaled off-band image. We adopted a similar method that fully exploits the information contained in the MUSE data cube: we first median-filtered the data cube in the spectral direction with a very wide filter window of ±100 spectral pixels; this produced a continuum-only cube with all line emission removed and with the continuum spectra of real objects being heavily smoothed. The Lyα image has been computed by choosing the band limits such that about 95 per cent of the total line fluxes were included. Being the Lyα nebula double peaked, the bandwidths resulted to be 14 and 9 spectral pixels (1pixel = 1.25 Å) for the blue and red Lyα peaks, respectively, corresponding to velocity width of 1300 km s^{-1} and 840 km s^{-1}. We then subtracted this filtered cube from the original data Lyα image and thus obtained an essentially pure emission line cube that was (to first order) free from any continuum signal. As an example, the $z = 1.037$ foreground galaxy has been optimally removed (see below). The spatial maps of the red, blue and 'red+blue' Lyα nebulae are shown in Fig. 1. The integrated Lyα flux computed within a polygonal aperture defined following the green contour of Fig. 1 is $(6.1 \pm 0.1) \times 10^{-17}$ erg s^{-1} cm^{-2} and $(4.4 \pm 0.1) \times 10^{-17}$ erg s^{-1} cm^{-2}, corresponding to 5.5×10^{42} erg s^{-1} and 4.0×10^{42} erg s^{-1} for the blue and red components, respectively.

4 RESULTS

4.1 Lyα emitting nebula in the UDF

When examining the Lyα emission of this nebula both spatially and spectrally, we identified two main characteristics.

(1) A double-peaked profile in the spectral domain, with blue and red components peaked at redshift 3.3172 and 3.3266 (and dv = 650 km s^{-1}), each one showing a blue/red tail. The bluer peak is more intense and broader than the red one (FWHM ∼520 ± 50 km s^{-1} and 280 ± 50 km s^{-1}, respectively).

(2) A different overall spatial distribution of the blue and red emission. From the corresponding spatial maps, it is evident that the bulk of the emission of the two peaks is segregated (marked with blue/red dotted circles of 1.2 arcsec diameter in Fig. 1). Again, the spectral shape of these two selected regions follows the profiles described above (the extracted one-dimensional spectra from the circular apertures are shown in the same figure), in which the strongest blue emission is also broader than the red one.

The ratio of the two peaks depends on the aperture adopted and the position on the nebula. For example, we identified two regions that show a deficit either of blue or red Lyα emission. These are marked with dotted ellipses in Fig. 1 (panels E and F). Further details of the spatial behaviour of the red and blue emissions along their spectral direction are shown in Figs 2 and 3, in which each slice with step of 1.25 Å is shown (dv = 70 km s^{-1}). In particular, the blue emission has been expanded in 13 slices from 5238.75 Å to 5253.75 Å and appears to grow first from the east side (where it is dominant, e.g. slice 4) and subsequently moves towards the west side following a non-uniform pattern, but maintaining a blue plume over the entire region (slices 10 and 11). The blue emission covers also regions where the red one is present. The average of all the slices within d$v \simeq$ 1300 km s^{-1} is shown in Fig. 2.

The red emission has also been expanded in 11 slices from 5255.0 Å to 5267.5 Å and is mainly located where its main peak has been identified (as discussed above), however in few slices it shows structures that extend towards the regions where the blue emission is dominant. The average of all the slices within dv$\simeq$ 840 km s^{-1} is shown in Fig. 3.

We map the Lyα emission spatially by extracting spectra from apertures covering different regions of the nebula. In particular, the one-dimensional profiles are shown in Fig. 4, where the two main emissions are shown with blue and red colours. Again, this clearly shows a broader blue component and the different intensities among the two red and blue peaks. It is worth noting that the nebula shows a double-peaked Lyα emission from both positions, 1 and 2, marking the blue and red dominant emissions (see Fig. 4). The wavelength

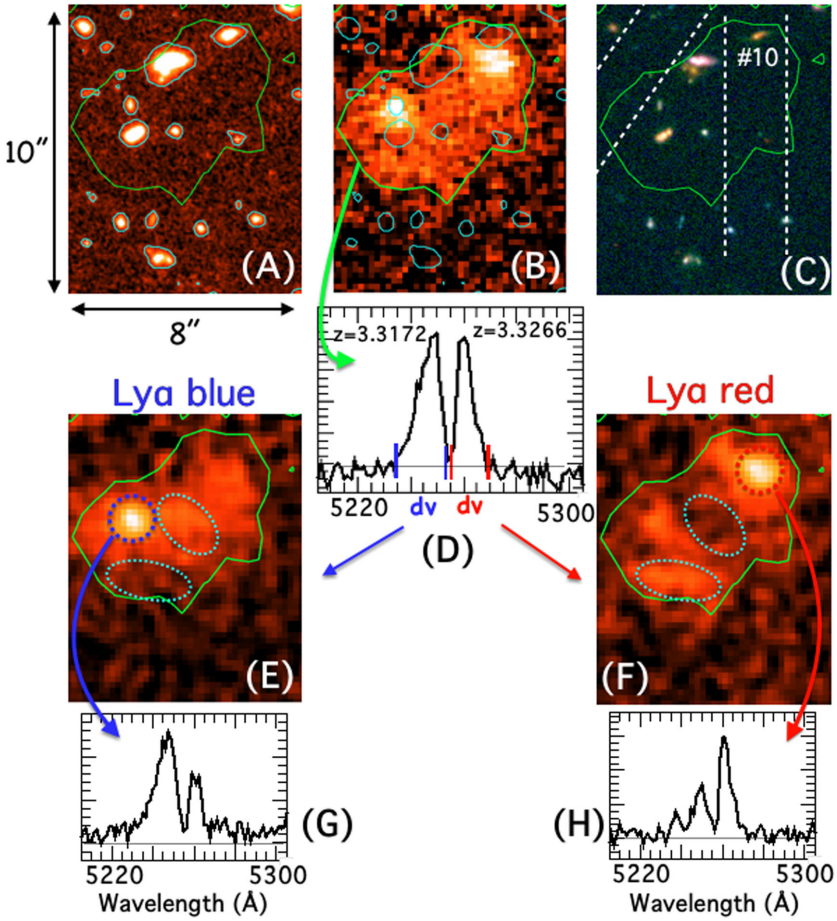

Figure 1. Panel A: *HST F*105*W*-band image of the region covering the Lyα nebula. Galaxies are highlighted with contours (only for eye-guidance). Panel B: Lyα nebula as the sum of the two Lyα peaks, blue and red. Contours indicate the position of galaxies, the green contour marks the Ly α emission above 2σ from the background. Panel C shows the colour image derived from the *HST*/ACS *F*435*W*, *F*606*W* and z850LP bands. The slit orientation of previous work by Rauch et al. (2011, 2016, dotted lines) and the galaxy no. 10 they discuss are indicated. Panel D: summed (red + blue) one-dimensional Lyα spectral profile integrated within the green contour, where two peaks are evident. The Lyα spatial maps of the blue and red components are shown in panels E and F), respectively. These are computed by collapsing the signal in the velocity intervals dv = 1300 and 840 km s^{-1} (marked with blue and red segments). Clearly, the blue and red peaks of the Lyα emission originate from two different, spatially separated regions. The Lyα one-dimensional spectra extracted over these two regions are shown in panels G and H. These spectra are extracted adopting circular apertures of 1.2 arcsec diameter (blue and red dotted circles). Dotted ellipses mark two regions over which each of the peaks of the Lyα emission either dominates or is depressed.

location of the Lyα trough is not changing significantly, remaining within d$\lambda \simeq 4$ Å (d$v \simeq 230$ km s^{-1}) from the central position (5255 Å, $z = 3.3226$), derived by integrating over the entire nebula (green contour in Fig. 4).

4.1.1 The broad-band counterparts

We discussed above about the spatial distribution and spectral profile of the emitting Lyα nebula. Here, we discuss the identification of possible broad-band counterparts. We were able to measure redshifts for 11 galaxies in the region surrounding the nebula, two of them – marked as no. 7 and no. 12 – with only tentative redshift estimates (see Fig. 5). The MUSE spectra are shown in Fig. 6, where the wavelength slices corresponding to the peak of the most prominent emission line are shown. The redshifts of these galaxies are in the range $1 < z < 6$. No X-ray emission has been detected from the 7Ms *Chandra* data, neither from the nebula nor from any of the galaxies close by, and no evident high ionization emission lines (e.g. C IVλ1548, 1550, He IIλ1640) have been identified. Given the non-detection and the flux limit of the *Chandra* 7Ms ($F_{0.5-2\,\mathrm{keV}} \simeq 4.5 \times 10^{-18}$ erg cm^{-2} s^{-1}, corresponding to $L_{2-10\,\mathrm{keV}} < 4 \times 10^{42}$ erg s^{-1} for a source at $z = 3.3$) we can definitely rule out the presence of a strong active galatic nucleus. We searched through all the available deep multiband photometry of the *HUDF*, finding no detection at any wavelength longer than the IRAC *Spitzer* channels (i.e. VLA, ALMA, *Herschel*, *Spitzer* MIPS 24 µm). This leaves us with the following 1σ upper limits:

(i) VLA 1.4GHz (21 cm): 0.5 µJy (Miller et al. 2013)
(ii) ALMA 1.3 mm: 120 µJy (Dunlop et al. 2016)
(iii) *Herschel* 100 µm: 0.8 mJy (Elbaz et al. 2011)
(iv) *Herschel* 160 µm: 2.4 mJy
(v) MIPS 24 µm: 20 µJy (Santini et al. 2009).

Several other galaxies show colours and photometric redshifts [from Coe et al. (2006) and CANDELS [2]] consistent with the redshift of the nebula and are reported in Fig. 1. Deep VLT/VIMOS *U*-band (Nonino et al. 2009) and *HST*/*F*336*W* (Rafelski et al. 2015) images are shown in Fig. 5. The dropout in these bands of several

[2] https://rainbowx.fis.ucm.es/Rainbow_navigator_public/

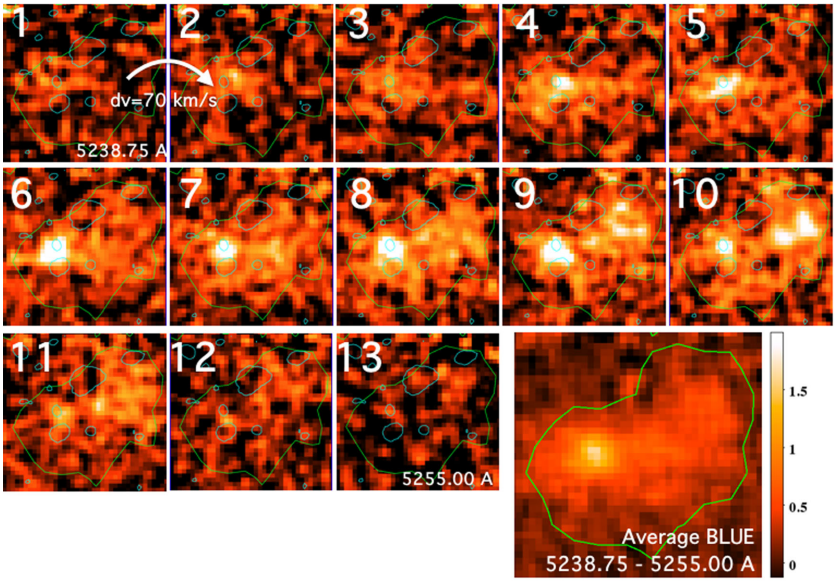

Figure 2. Unpacked images of the blue Lyα component in 13 slices of 1.25 Å each. The images are sorted by progressively increasing wavelength from top-left to bottom-right spanning the range 5238.75 Å–5255.00 Å. Cyan contours highlight the position of galaxies as shown in Fig. 1. A dominant emission is present on the left (east) with an arising plume towards the right-hand side (west) as wavelength increases. In the bottom-right panel, the average of the all slices is shown. The green line indicates the Lyα nebula contour from the 'red+blue' map. The colour-coded bar indicates units of 10^{-20} erg^{-1} s^{-1} cm^{-2} pix^{-2}, with 1pix = 0.2 arcsec.

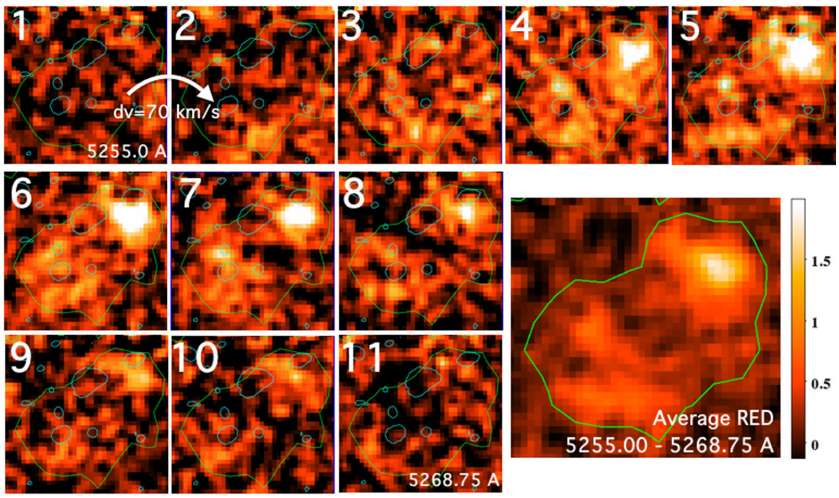

Figure 3. Unpacked images of the red Lyα component in 11 slices of 1.25 Å each. The images are sorted by progressively increasing wavelength from top-left to bottom-right spanning the range 5255.00 Å–5268.75 Å. Cyan contours highlight the position of galaxies as shown in Fig. 1. A dominant emission is present on the right (west) with structure extending towards the left-hand side (east). In the bottom-right panel, the average of the all the slices is shown. The green line indicates the Lyα nebula contour from the 'red+blue' map. The colour-coded bar indicates units of 10^{-20} erg^{-1} s^{-1} cm^{-2} pix^{-2}, with 1pix = 0.2 arcsec.

galaxies further supports their high-redshift nature. We confirm the presence of a foreground galaxy at $z = 1.037$ and find five additional sources at $z > 3.7$, which are certainly not associated with the nebula. The position of a group of galaxies at zphot $\simeq 2.5$ is also marked in the figure. One of them is spectroscopically confirmed at $z = 2.4462$. As expected, they are also detected in the VIMOS U-band. Three galaxies (namely, no. 3, no. 4 and no. 6) have spectroscopic redshifts within d$z = 0.23$ (corresponding to dv<16 000 km s^{-1} or <50 Mpc proper) from the red or blue Lyα emissions (all redshifts are reported in Figs 5 and 6). While galaxy no. 3 has a redshift very close to that of the nebula and is very likely physically connected to it (see Section 4.1.2), galaxy no. 4 and no. 6 have redshift differences of $z_{\rm nebula} - z_{\rm gal} = 0.13$ and 0.23, respectively. This places them relatively far in front of the nebula (at $\simeq$27 and 49 Mpc proper, respectively). However, these two galaxies could still contribute to the fluorescence of the nebula if there is escaping ionizing radiation arising from them with wavelength bluer that 884 Å and 862 Å, respectively (due to the Hubble flow, redder photons become non-ionizing at those distances). Indeed, the mean free path of ionizing radiation at $z = 3$ is $\sim$100 Mpc proper (Worseck et al. 2014). So, it is still possible for the ionizing radiation from a galaxy at these distances to reach the nebula.

We were not able to confirm the redshift reported by Rauch et al. (2011, 2016) for the galaxy no. 10, at $z = 3.344$; in particular,

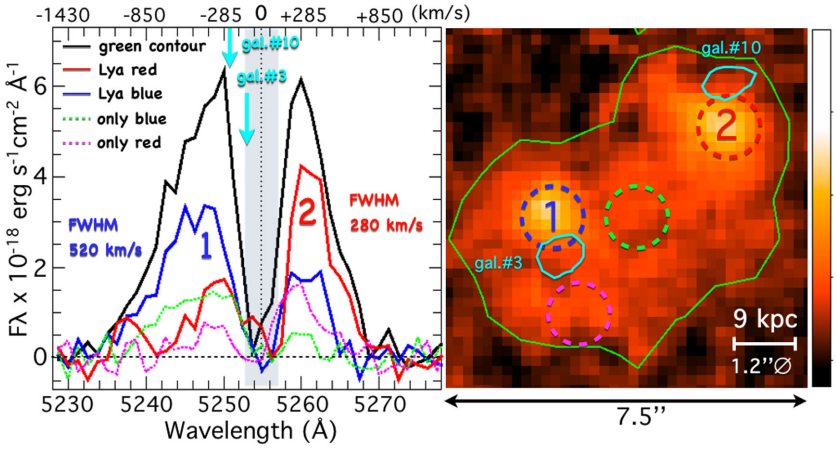

Figure 4. Right-hand panel: the position of four circular apertures (1.2 arcsec diameter) is shown on the image of the Lyα nebula (the image shown here is 'red+blue'). Green and cyan lines mark the contour of the nebula and galaxies (as described in Fig. 1). The two apertures centred on the dominant emissions (1 and 2) are shown in blue and red on the left-hand panel. The galaxy LBGno. 3 is marked with a thick cyan contour and its velocity position relative to the nebula is shown in the left-hand panel. Left-hand panel: the one-dimensional Lyα profiles extracted from the apertures are indicated on the right-hand panel. In particular, the total profile (extracted from the green contour) is shown in black, and the spectra arising from the apertures 1 and 2 on top of the main emissions are shown in blue and red, respectively (the FWHM are also indicated). Dotted magenta and green lines mark the Lyα profiles in regions where the blue and red emission are deficient, respectively. In general, the double-peaked Lyα emission persist over the nebula with the position of the trough consistent with the marked grey region, $\simeq$230 km s^{-1} wide.

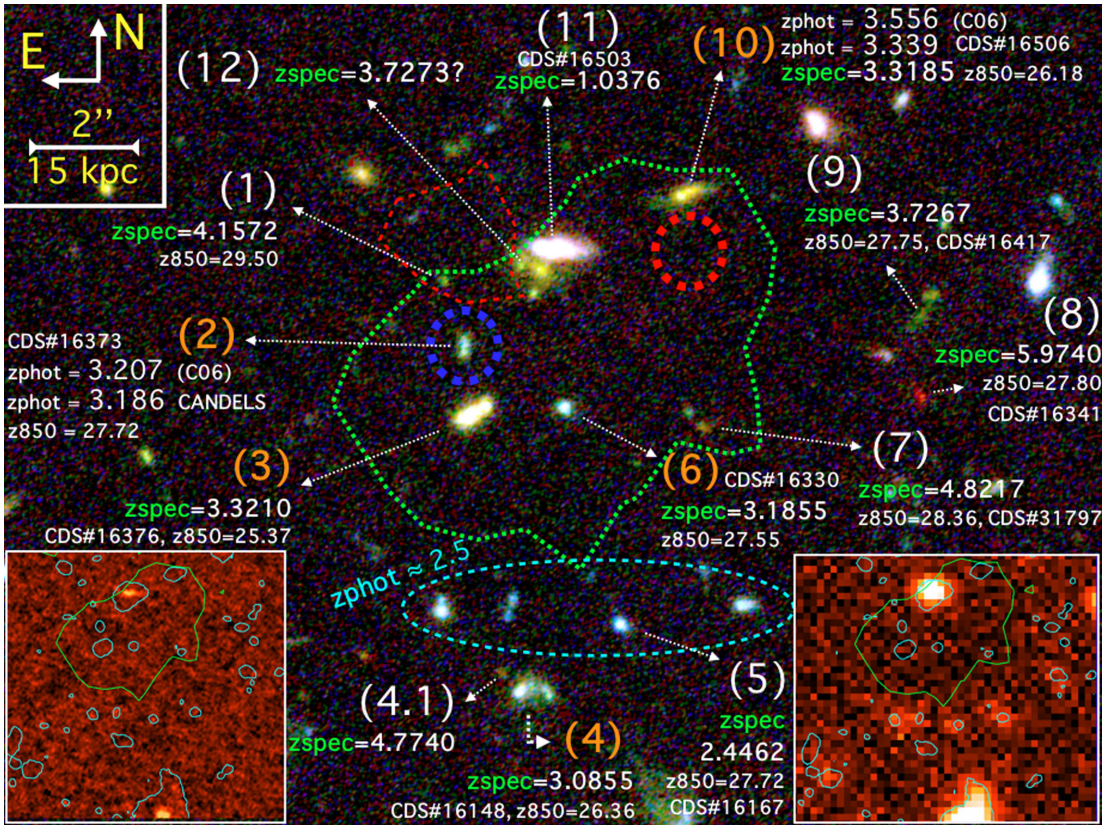

Figure 5. Galaxies surrounding the Lyα nebula (dotted green contour) are shown superimposed to the *HST* colour image centred on the nebula (*F*435*W*, *F*606*W* and i775*W*, Beckwith et al. 2006). Dashed red and blue circles mark the positions of the dominant Lyα red and blue emissions, respectively (see also Fig. 1, panel B). Redshifts extracted from MUSE are highlighted in green and z_{850} magnitudes derived from Coe et al. (2006). The CANDELS identifier is also reported (CDSno.) for relevant sources (in particular the IDs highlighted in orange are galaxies spectroscopically confirmed at redshift close to the nebula, see text). The photometric redshifts are reported, if no reliable features were found in the MUSE data cube (Coe et al. 2006 and CANDELS). The two insets on the lower corners of the figure show the same region of the sky in the deep *F*336*W* (left) and U-VIMOS (right) bands. This highlights the drop of the majority of the sources considered in this study, therefore supporting their high-redshift nature, $z \gtrsim 3$. Galaxies close to the nebula are marked in orange, in particular galaxy ID = 3 lies in the Lyα trough (see text). The thin-dotted red contour marks a possible Lyα halo at $z = 3.723$, shown in the bottom-left panel of Fig. 6.

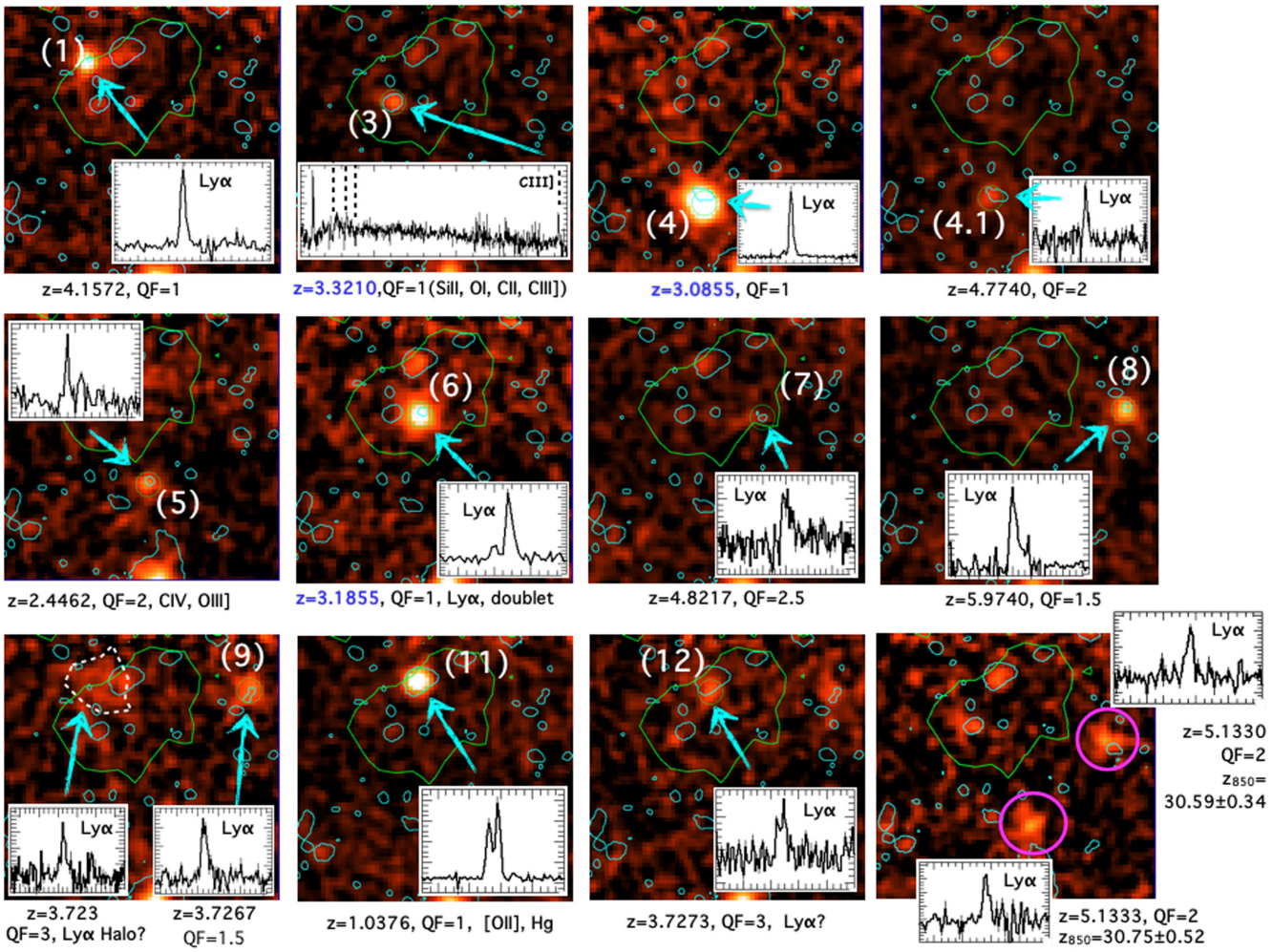

Figure 6. Snapshots of the MUSE spectra (dλ = 1.25 Å) of the identified lines. The IDs correspond on the galaxies marked in Fig. 5 following from top-left to bottom-right the counterclockwise order. Redshifts are reported in the bottom of each image, with the quality (QF, 1 = secure, 2 = plausible, 3 = tentative) and the main spectral feature identified. In the bottom-right, two emission lines not associate to any CANDELS source are reported. They are consistent with the position of two sources identified by Coe et al. (2006), with magnitudes $z_{850} \gtrsim 30.5$.

we do not detect the He IIλ1640 emission line at the redshift they reported. Rauch et al. (2016) measured the redshift using *HST* grism spectroscopy (within the GRAPES survey; Pirzkal et al. 2004) that has only modest spectral resolution $R \sim 100$ (a factor of >20 smaller compared to MUSE) therefore subject to larger uncertainties. For this reason, we allowed for a larger spectral window when searching for this feature in the MUSE data. The MUSE spectrum in the expected position of He IIλ1640 is free from sky lines (see Fig. 7), and does not show evident line emission down to 3×10^{-18} erg s^{-1} cm^{-2} at 3σ level, assuming an emission line with FWHM $\simeq$ 100 km s^{-1}. Although not highly significant, it is worth noting a possible broad emission around ∼7124 Å, that interestingly, if true, could be interpreted as broad He IIλ1640 produced by Wolf–Rayet stars. However, this feature is not significant enough to allow us to explore this scenario any further.

In order to try to optimize the S/N and hence improve the detection of faint spectral features, we have extracted spectra from different apertures (from 0.4 arcsec to 1.2 arcsec) from the MUSE cube around the position of galaxy no. 10. Since the prominent Lyα visible in all the extracted spectra could be associated with the extended nebula, rather than to the galaxy itself, we tried to measure a redshift based only on the spectral shape of the continuum, therefore excluding the Lyα emission line. We masked the Lyα emission and performed a cross-correlation with several spectral templates of star-forming galaxies with no Lyα in emission (we used the typical Lyman break galaxy spectra, i.e. Shapley et al. 2003; Vanzella et al. 2009). In this way, while the continuum break at 5230–5315 Å is very clear, the absence of evident UV absorption (or emission) lines still prevents us from deriving a precise redshift measurement. The best solution we find, when cross-correlating with templates and when excluding the Lyα line, is $z = 3.3180$. If the Lyα is not masked, we obtain $z = 3.3185$. In the latter case the redshift is mainly based on the Lyα emission line. However, we cannot determine if the Lyα is associated with the galaxy or if it is simply part of the extended nebula intersecting the line of sight (los). The only possible additional feature we find in the MUSE spectra is C III] λ1908 at $z = 3.3185$. Therefore, again at the same redshift of the Lyα nebula. To help visualizing this additional emission line, we produced a pseudo long-slit 2D spectrum, by co-adding the MUSE spaxels within a rectangular region mimicking a slit with 1 arcsec width and the same orientation was adopted by Rauch et al. (2016). This is shown in Fig. 7 and it supports the detection of C III] λ1908 in the one-dimensional spectrum.

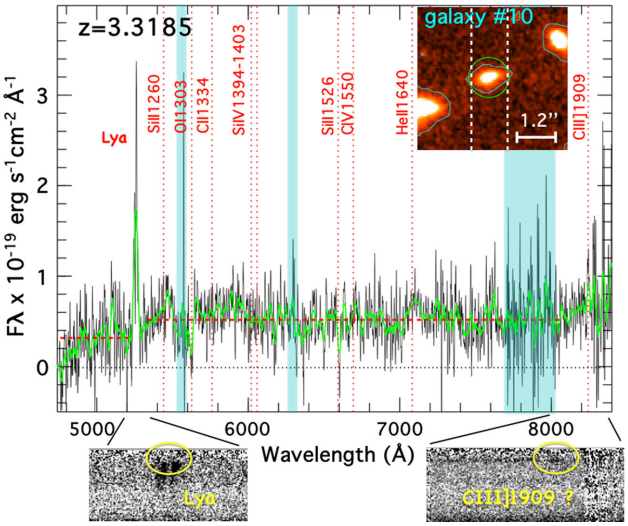

Figure 7. The MUSE spectrum of galaxy no. 10 calculated within a 1.2 arcsec diameter aperture (green circle in the inset) is shown. The black and green spectra are smoothed with a Gaussian filter of 2 and 10 pixels standard deviation, respectively. Vertical cyan stripes indicate zones of intense sky emission lines. The two insets in the bottom show the two-dimensional spectra around the Lyα and C III] λ1908 regions, obtained simulating a long-slit spectroscopy with slit width and orientation as marked in the top-inset, white dashed line. While no evident absorption lines have been detected, the possible C III] $\lambda\lambda$1907, 1909 in emission and the clear continuum break (marked with dashed red line) are fully compatible with the Lyα emission of the nebula (see text for more details).

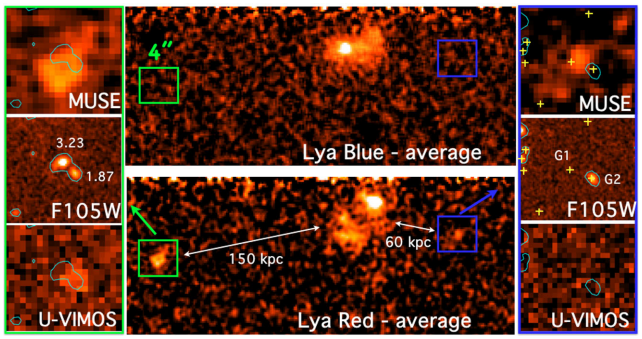

Figure 8. The position of additional Lyα emissions placed at a transverse distance of 150 kpc and 60 kpc proper from the nebula is shown. In the middle top/bottom panels, the blue/red emission of the nebula averaged within the velocity slices reported in Fig. 1 is shown with the marked additional Lyα emissions. The emissions marked with a green and blue squares at the same wavelength of the red Lyα nebula are evident. In the left-hand and right-hand panels, a zoom of these emissions is shown: from top to bottom, the zoomed Lyα emission, the *F*150*W* image (with indicated the photometric redshifts from Coe et al. 2006) and the deep U-VIMOS image are shown. Cyan contours mark the position of the galaxies as indicated in Fig. 1. In the left-hand panels, a galaxy with photometric redshift consistent with the Lyα emission has been identified (zphot = 3.23), while the second lower-z object (zphot = 1.87) is also detected in the VIMOS *U*-band (bottom-left image). In the right-hand panels, the positions of sources detected in the Coe et al. (2006) catalogue (yellow crosses) are also shown. In particular, galaxy G1 and G2 have photometric redshifts $z \simeq 3$ and magnitude in the z_{850}-band of 30.80 (S/N = 2.8) and 28.81 (S/N = 14), respectively.

While the galaxy is a clear *U*-band dropout with photometric redshifts 3.556 (Coe et al. 2006) and 3.339 (CANDELS), and consistent with the other galaxies and nebula discussed here, we consider the redshift still uncertain. Although we were not able to obtain a clear redshift measurement for this galaxy, we decided to report our redshift estimate obtained with the method described above, $z = 3.3185$, which we classify as 'plausible' and to which we assign a quality flag QF = 2. The MUSE spectrum of this galaxy is shown in Fig. 7.

We noted another galaxy presenting a multiblob morphology, close (<0.3 arcsec) to the $z = 1.037$ foreground galaxy and towards the south-east. This object is not recovered by any public photometric catalogue, neither CANDELS (Guo et al. 2013) nor GOODS-ACS (Giavalisco et al. 2004). Additionally, this 'multiblob' object is a *U*-band dropout, as can be inferred from the high spatial resolution deep *HST*/*F*336*W*-band imaging, therefore it is plausibly at $z \gtrsim 3$. We tentatively identified an emission line at 5747 Å that, if interpreted as Lyα, would place the source at $z = 3.727$. Interestingly, the emission appears spatially resolved suggesting it could be another Lyα blob behind the $z = 3.2$ nebula discussed here (this putative blob is marked with a dotted line in Figs 5 and 6). Another galaxy (no. 8) has been confirmed at the same redshift ($z = 3.7267$) of this second blob. When focusing on this $z = 3.7$ emission superimposed on the *HUDF* nebula, another Lyα nebula emerges at 11 arcsec from it, in the south-east at $z = 3.7123$ with extension 30 × 20 kpc physical. We do not discuss further this projected higher redshift Lyα haloes, neither the second system at 11 arcsec, and focus on the $z = 3.2$ nebula.

The two-dimensional MUSE snapshots (slices of 1.25 Å bin) at the wavelength of the main peak of the identified lines are shown in Fig. 6, together with their one-dimensional zoomed spectra. The reported IDs are the same as in Fig. 5. In general, line emissions are evident and the spectral resolution ($R \simeq 1800$) is sufficient to detect the low redshift [O II] λ3727, 3729 doublet (e.g. galaxy no. 11, other than Hγ) and the asymmetric profile typical of the high-z Lyα lines. Only for one galaxy (no. 3, the brightest with $z_{850} = 25.37$) the continuum and several absorption lines have been identified together with the C III] $\lambda\lambda$1907, 1909 emission (this emission is shown in Fig. 6). Interestingly, two more line emitters have been identified at the same wavelength and associated with two faint galaxies identified by Coe et al. (2006) with magnitude $z_{850} = 30.59 \pm 0.34$ and 30.75 ± 0.52 (detected at 2σ and 3σ, respectively; they are shown in the bottom-right panel of Fig. 6). The lines are reasonably well detected (S/N∼5–7). One of the two is possibly asymmetric resembling the typical Lyα shape. If the lines are Lyα at $z = 5.133$, they are obviously not associated with the system studied in this work. However, the detection of such a faint spectral feature from galaxies that are so faint to be barely detected even at the *HUDF* depth, further supports the capability of the MUSE instrument of detecting possible faint counterparts also at the redshift of the nebula.

It is worth noting other two Lyα emissions identified at ≃150 kpc and 60 kpc proper from the nebula and at the same redshift of the red Lyα component. Fig. 8 shows the positions of these emissions compared with the position of the underlying galaxies, whose photometric redshift is also reported. These additional emission lines are consistent with the photometric redshifts of the closest galaxies, whose magnitudes ranges between 27 up to 30.8 in the z_{850} band. The Lyα emission appears slightly spatially offset from the reported galaxies, possibly due to radiative transfer effects (see Fig. 8).

In the following, we focus on the closest galaxies possibly related to the Lyα system.

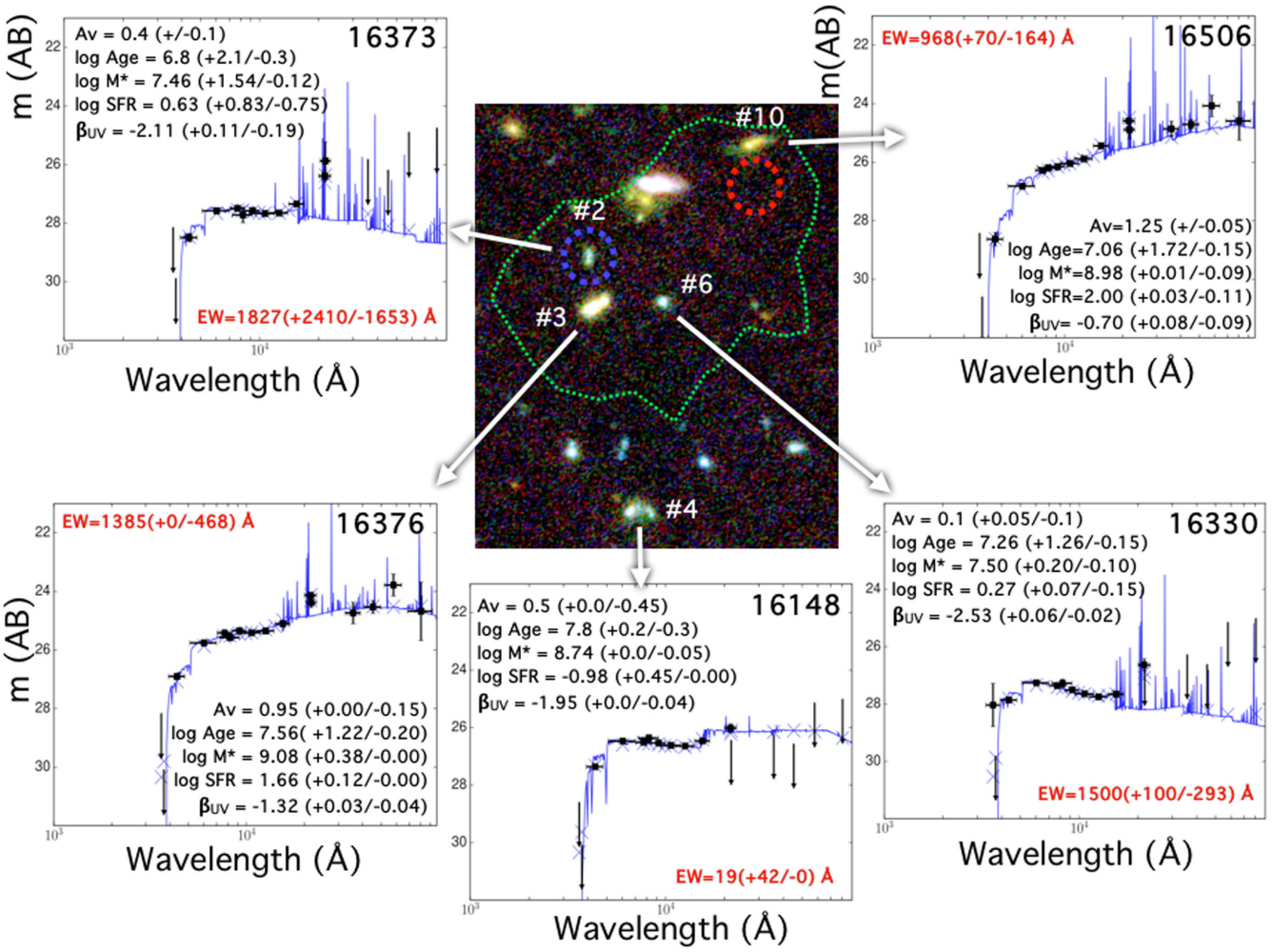

Figure 9. The SED-fitting of the galaxies described in the text and possibly associated with the nebula are shown. The IDs are same used in the previous figures and Table 1. Basic physical quantities are reported in black, while the estimated equivalent width of the group [O III] λλ4959, 5007 and Hβ is reported in red. Apart from galaxy no. 4, all the other galaxies show very high equivalent widths. In particular, galaxy no. 4 is the bluest one of the sample, consistent with a negligible dust attenuation

4.1.2 The dominant blue and red Lyα emissions and galaxy counterparts

Three galaxies have been spectroscopically confirmed at redshift 3.3210 (no. 3), 3.1855 (no. 6) and 3.0855 (no. 4) at <4 arcsec from the main blue emission of the nebula, corresponding to few proper kpc transverse (1 arcsec = 7.6 kpc proper). Another galaxy, no. 10, has been plausibly confirmed at redshift 3.3185 close to the red emission. We describe them more in detail in the following.

(i) *galaxy no. 3.* Given its redshift ($z = 3.3210$), this is the galaxy that is closest to the nebula in the velocity space with a $dz = 0.0016$ from the estimated Lyα trough, corresponding to $dv \simeq 110$ km s^{-1} in the rest frame of the nebula. This galaxy is spatially resolved and shows a well-detected continuum with several ultraviolet low-ionization absorption lines in the MUSE spectrum, e.g. [Si II] λ1260, [O I] λ1303 and [C II] λ1334 (see Figs 5 and 6). The estimated stellar mass is 1.2×10^9 M$_\odot$ with a star formation rate of 46 M$_\odot$ yr^{-1} (the resulting physical parameters are reported in Fig. 9). The C III] λ1908 emission has also been detected and provides an estimate of the systemic redshift that is fully compatible with the trough of the Lyα nebula (see Fig. 4). Given the redshift and the angular separation from the main blue Lyα peak (1 arcsec), this galaxy is the closest spectroscopically confirmed source located at a few tens of physical kpc from the Lyα system. Interestingly, this galaxy is well detected in the HAWKI-Ks band (Fontana et al. 2014) with a magnitude 24.13 at S/N ≃ 40, about 1.0 and 0.6 mag brighter than the adjacent *HST*/*F*160*W* and *Spitzer*/IRAC 3.6μm bands with magnitudes 25.10 and 24.73 detected at S/N ≳ 40 and S/N ≃ 3, respectively. This discontinuity in the *K*s-band strongly suggests the presence of intense [O III] λλ4959, 5007 and H β nebular emission lines (see the best SED fitting in Fig. 9). Indeed, the result from the SED fitting including nebular prescription produces the best solution with a total equivalent width of EW([O III] λλ4959, 5007+ Hβ) = 1000 Å. Interestingly, the relatively weak interstellar absorption lines (especially [C II] λ1334) the C III] λ1908 emission, and the strong optical rest-frame Oxygen emissions traced by the broad-band *K*s magnitude, resemble the properties recently identified by Vanzella et al. (2016) in a Lyman continuum emitter at a similar redshift $z = 3.2$ (see also de Barros et al. 2016). In Section 5, we discuss in more detail the possible link between escaping ionizing radiation and the surrounding gas, in particular via fluorescence.

(ii) *galaxy no. 6.* This is a rather faint ($z_{850} = 27.55$), compact, and low-mass galaxy with stellar mass 3.2×10^7 M$_\odot$ showing an extremely blue ultraviolet slope ($\beta = -2.55$). The SED fitting

suggests a low dust extinction, $A_v = 0.1$, an SFR $= 0.3\,M_\odot\ yr^{-1}$. The prominent Lyα emission is consistent with the young ages inferred for the burst (10^7yr). The Lyα line also shows a relatively narrow double-peaked separation ($dv \simeq 400\,km\ s^{-1}$) if compared to the brighter $L^\star$ galaxy counterparts of Lyα nebulae (e.g. Kulas et al. 2012). The small peak separation observed in this source is more in line with recent findings at fainter luminosities, where optically thin systems have been identified (Karman et al. 2016; Vanzella et al. 2016). Given its measured redshift ($z = 3.1855$), this galaxy might be located in front of the Lyα system. Interestingly, galaxy no. 6 is positioned over the region where the red emission is minimal, while the blue still survives (see dotted ellipse in Fig. 1).

(iii) *galaxy no. 4.* This is another galaxy with prominent Lyα emission at $z = 3.0855$ (see Fig. 6), identified towards the south, at <4 arcsec from the nebula. The inferred stellar mass is $5.5 \times 10^8\,M_\odot$ with an SFR$\simeq 0.1\,M_\odot\ yr^{-1}$ (see Fig. 9).
The redshift difference between the galaxy and the Lyα trough is $dz = -0.237$ and corresponds to $-16\,400\,km\ s^{-1}$. Therefore this galaxy appears to be located in front of the system.

(iv) *galaxy no. 2.* It is worth noting that the blue Lyα peak is exactly aligned with another faint galaxy with magnitude $z_{850} = 27.72$ (galaxy no. 2, marked in Fig. 5), for which no spectroscopic redshift has been measured from MUSE, unless the strong blue Lyα emission of the nebula contains also the Lyα of the galaxy. Unfortunately, it is not possible to clarify this issue with the current data. The photometric redshift is, however, very close to the redshift of the nebula and the estimated stellar mass is $3 \times 10^7\ M_\odot$ and young age $\simeq 10^{7-8}$ years, with a relatively blue ultraviolet slope (see Fig. 9). As in the case of galaxy no. 3, discussed above, this galaxy has also been detected in the *K*s-band (with S/N = 6) and it appears one magnitude fainter in the *F*160*W* band, while only upper limits are available in the IRAC/3.6 μm and 4.5 μm channels $m > 26$. The presence of intense nebular emission lines ([O III] λλ4959, 5007 and Hβ) is, therefore, expected also in this galaxy. When quantified through the SED fitting, the nebular emission lines should have EW = 1800 Å (see Fig. 9). While a confirmation would need dedicated near-infrared spectroscopy, such strong nebular emission lines are suggestive of high ionization parameters and possible Lyman continuum leakage (e.g. de Barros et al. 2016).

(v) *galaxy no. 10.* The main red peak of the nebula has no obvious aligned counterparts. As already discussed above, the closest galaxy is that reported by Rauch et al. (2011, 2016), here identified as galaxy no. 10, for which we were not able to confirm Rauch et al. (2016) redshift, based on He IIλ1640 detection at $z = 3.344$ ($\lambda \simeq 7124$ Å). As already discussed above, Fig. 7 shows the MUSE spectrum where no clear emission lines have been detected at $\lambda \simeq 7124 \pm 30$ Å down to $\simeq 3 \times 10^{-18}\ erg\ s^{-1}\ cm^{-2}$ at 3σ level (a region free from sky emission lines). The position of relevant ultraviolet lines is marked with dotted vertical lines in Fig. 7. Rather, looking more carefully at the MUSE spectrum a continuum break is detected across the Lyα emission. It is not clear if the Lyα (double-peaked) emission is coming from the galaxy or is the effect of the seeing that spreads the signal into the adopted circular aperture when extracting the MUSE spectrum (marked with a green circle in the inset of Fig. 7). The cross-correlation with typical LBG templates (e.g. Vanzella et al. 2009) including/excluding the Lyα line produces the following solutions, $z = 3.3185/3.3180$, respectively (the $z = 3.3185$ would also be compatible with possible C III] λ1908 line emission). In both cases, the redshift is slightly lower than reported by Rauch et al. (2016) and places the galaxy at $\simeq -285\,km\ s^{-1}$ from the Lyα trough of the nebula, while the previous redshift, $z = 3.344$, would put it at $+1480\,km\ s^{-1}$, redder than the red peak of the nebula. As discussed by Rauch et al. (2011, 2016) this galaxy together with the other counterparts is probably playing a role in shaping the profile and morphology of the Lyα nebula. We performed SED fitting also for this galaxy, obtaining a remarkable star formation activity ($\sim 100\,M_\odot\ yr^{-1}$) with a stellar mass of $\simeq 10^9\,M_\odot$ (the more massive among the counterparts) and relatively red ultraviolet slope (Fig. 9).

4.2 Gravitationally lensed Lyα emitting nebula in the Hubble Frontier Fields MACS J0416

Another strongly magnified Lyα nebula has been discovered at redshift $z = 3.22$ behind the Hubble Frontier Fields MACSJ0416, as a gravitationally lensed system showing two multiple images (see Fig. 10). We report about this system because of its very similar spectral properties to the nebula discovered in the *HUDF*. We refer in particular to the very similar Lyα emission line profile that is also double-peaked and shows a blue peak more prominent than the red one. The size of the modelling emitting gas is smaller than the system discovered in the *HUDF*, having a lens-uncorrected (i.e. observed) extension of the order of 40 kpc. The two images have been identified at RA = 04h16m10.9s, DEC = −24°04′20.″7 (the more magnified image, image A hereafter, with magnification $\mu \simeq 2$) and RA = 04h16m09.6s, DEC = −24°03′59.″7 (a second less magnified image, image B hereafter, with $\mu \simeq 1$). This multiple imaged system has been used in the new highly precise strong lensing model that uses a large set of new multiple systems spectroscopically confirmed with MUSE (it corresponds to System 9 in Caminha et al. 2016). The image positions are fully consistent with the strong lensing model that accurately reproduces their positions. The morphology in the source plane is slightly distorted, but a more careful dedicated modelling would be required to derive meaningful conclusions. That is out of the scope of this work and it will be presented in a separate dedicated study (Caminha et al. 2016). We note that also in this case the spatial distribution of Lyα-red and Lyα-blue (especially in image A) is not coincident. This is shown in Fig. 10, where the red contours mark the position of the Lyα-red emission, which appears slightly displaced compared to the Lyα-blue emission.

Remarkably, the spectral properties of this nebula are very similar to those of the *HUDF* nebula discussed above. In particular, the (1) rest-frame velocity difference, (2) line widths (FWHM), and (3) global shape – e.g. the bluer Lyα peak is systematically broader than the red one – are very similar in both nebulae. Fig. 11 shows a comparison of the two spectral profiles as they are observed. After correcting the line fluxes by the magnification factor (e.g. $\mu = 2$ for image A), we obtain a Lyα luminosity of 4.4×10^{42} erg s^{-1} and 3.7×10^{42} erg s^{-1} for the blue and red peaks, respectively. The relative peak ratio changes as in the *HUDF* nebula, showing different regions where either the blue or the red emission dominate.

The multiple images produced by strong lensing allow us to investigate the broad-band counterparts more easily than in the *HUDF* case. In particular a triplet of galaxies aligned with the emitting gas (Lyα) have been identified. They are visible in both multiple images (A and B) and, therefore, are likely associated with the nebula. If they were at a different redshift, no multiple images would be produced or they would be significantly offset from the Lyα emission (see Fig. 10). It is worth noting that also in the strongly lensed Lyα blob studied by Caminha et al. (2015) there were three aligned star-forming galaxies associated with the emitting gas. The clear double-peaked spectral shape of the Lyα emission showing blue and red asymmetries suggests it is not the simple sum of the

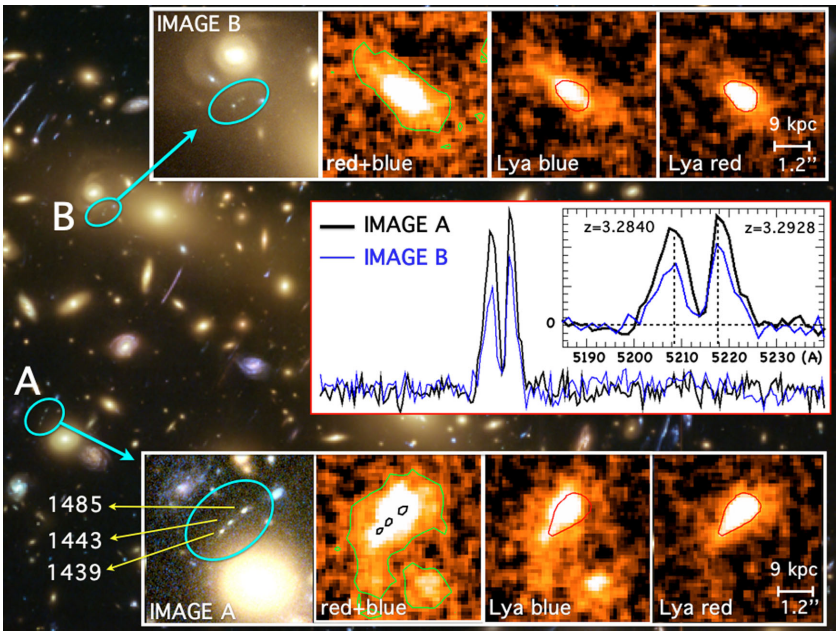

Figure 10. The lensed Lyα nebula discovered behind the Hubble Frontier Field MACSJ0416 at $z = 3.2$ is shown. Two multiple images have been marked and Lyα spatial distribution is shown in the insets (from left to right: the colour image, Lyα 'red + blue', only red and only blue). In the middle inset, the spectrum around the Lyα and a zoomed spectral profile are shown for both images, A (thick black line) and B (thick blue line). The three galaxies associated with the nebula are marked in the bottom left with yellow arrows and the corresponding IDs from the ASTRODEEP catalogue (Castellano et al. 2016).

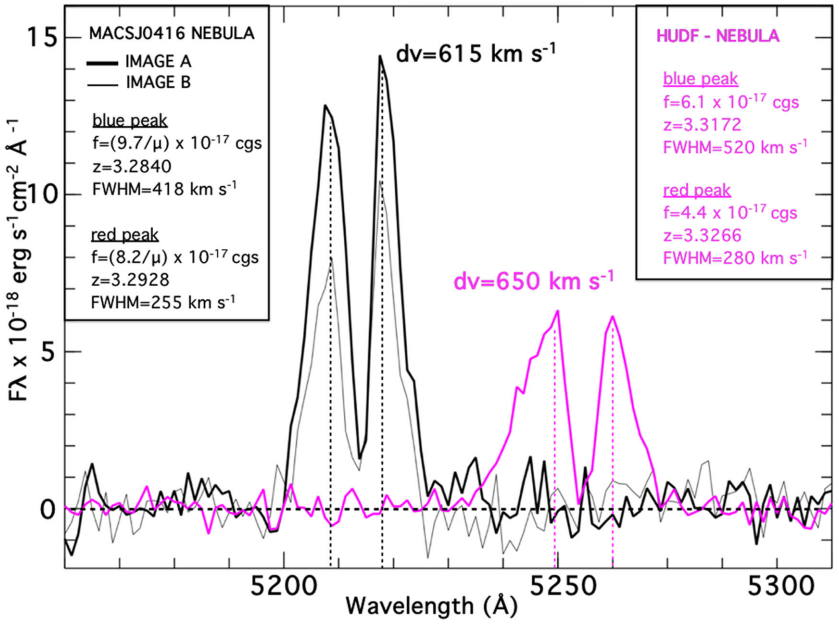

Figure 11. The two Lyα profiles of the nebulae described in this work are shown in the observed wavelength domain. Black thick (thin) line shows the profile for the lensed nebula, image A (B). Relevant parameters are reported. In the case of MACSJ0416 nebula numbers are reported for image A, for which the magnification is $\mu \simeq 2$ (Caminha et al. 2016). Remarkably, the trough, velocity difference, and widths of the two nebulae are very similar.

Lyα emissions arising from each galaxy and blurred by the seeing in the MUSE image. Rather, it appears as a diffuse well-resolved emission of $\simeq$4.0 × 2.5 arcsec (in the case of image A) detected in a region much larger than the stellar continuum of each galaxy (see black contours in Fig. 10).

Other than the Lyα emission, no additional spectral feature (e.g. no high ionization lines, C IVλ1548, 1550, O III] λ1661, 1666, C III] λλ1907, 1909 has been identified in the spectra of these galaxies. Therefore, we assume that these three galaxies are at the redshift of the nebula on the basis of geometrical arguments, and with the support of the lensing model. We checked the photometric redshifts of the three galaxies using the ASTRODEEP photometric redshift catalogue recently published by Castellano et al. (2016). All of them are fully consistent with the redshift of the Lyα nebula, $z = 3.2$. More specifically, the three galaxies have ASTRODEEP IDs 1439, 1443 and 1485 and photometric redshift $\simeq$ 3.55, 3.35 and 3.45. Two of them, 1439 and 1443, show relatively low stellar mass $4.4/\mu \times 10^8$ $M_\odot$ and $3.0/\mu \times 10^9$ $M_\odot$ and a possible excess in

the *K*-band that would suggest a strong nebular contribution in this band by the group of lines [O III] λλ4959, 5007 + Hβ. As discussed above, these features may suggest a possible link with escaping ionizing radiation. The third galaxy, 1485, is the most massive one with $1.5/\mu \times 10^{10}\,M_{\odot}$.

The star formation rate of the three objects (1439, 1443 and 1485) has been estimated to be $1.5/\mu$, $1.2/\mu$ and $3.4/\mu$ $M_{\odot}$ yr^{-1}, respectively, and $\mu \simeq 2$ (Castellano et al. 2016).

5 DISCUSSION AND CONCLUSIONS

We presented two extended Lyα systems at redshift ≃3.3. The prominent blue peak in their Lyα spectra accompanied by a fainter red, slightly narrower peak is remarkable (to our knowledge similar systems have been rarely identified at high redshift, $z \gtrsim 3$, e.g. Kulas et al. 2012). Usually, Lyα has been observed with dominant red tails indicative of outflows (e.g. Shapley et al. 2003; Vanzella et al. 2009) as well as many Lyα blobs (e.g. Matsuda et al. 2006). Here we observe the opposite. This is even more relevant if the intergalactic absorption is considered, that would tend to preferentially suppress the bluer peak. In particular, an IGM transmission in the blue side of the Lyα ranging between 20 per cent and 95 per cent (68 per cent interval) with a mean of ∼80 per cent has been proposed by Laursen, Sommer-Larsen & Razoumov (2011).

The Lyα nebulae described in this work benefit from the integral field spectroscopy (MUSE), which is more informative than previous long-slit studies (e.g. Rauch et al. 2016). Despite that, the complexity of the system still prevents us from deriving firm conclusions. So, we can at best test the plausibility of the processes involved and discuss the most likely scenarios.

As mentioned above, the nebulae described in this work show a quite complex structure with spatial-dependent Lyα emission (Figs 2 and 3) and varying sub-spectral profiles (Fig. 4); however, two clear spectral features are present in both systems: (1) the broad doubled-peaked line profile with prominent blue emission and (2) the 'trough' separating the two peaks that appears to occur mostly at the same frequency throughout the nebula (this is best illustrated by the *left-hand panel* of Fig. 4). These two observations combined can be naturally explained with scattering, and support the fact that radiative transfer effects are likely responsible for shaping the spectra emerging from these nebulae.

The simplest version of the scattering medium consists of a static gas cloud of a uniform density. For such a medium, the emerging Lyα spectrum is double peaked, with the peak separation set by the total H I column density of the cloud (e.g. Harrington 1973; Neufeld 1990; Dijkstra 2014):

$$N_{H\,I} = 5.3 \times 10^{20} \left(\frac{T}{10^4\,\mathrm{K}}\right)^{-1/2} \left(\frac{\mathrm{d}v}{670\ \mathrm{km\ s^{-1}}}\right)^{3} \mathrm{cm^{-2}}. \quad (1)$$

However, this possibility has been excluded by Rauch et al. (2011) on the basis of similar spectral properties we find here, e.g. the relatively stronger intensity of the blue versus red emission and the different widths suggests that we are not observing a static configuration. Radiative transfer through clumpy/multiphase media can also explain double-peaked spectra (see Gronke & Dijkstra 2016). Clumpy media generally give rise to a wide variety of broad, multipeaked spectral line profiles. The trough at a constant frequency then reflects either that there is a non-negligible opacity in residual H I in the hot inter clump gas (Gronke & Dijkstra 2016), or in the cold clumps that reside in the hot halo gas (the presence of these clumps inside massive dark matter haloes has been proposed by, e.g. Cantalupo et al. 2014 and Hennawi et al. 2015). The width of the trough reflects either the thermal broadening of the Lyα absorption cross-section for residual H I in the hot gas, and/or the velocity dispersion of the cold clumps.

Also the origin of Lyα emission in these nebulae is not easily identifiable.

Star formation. The association of the brightest Lyα spots with galaxies (in the *HUDF* nebula) and the three aligned star-forming galaxies in the lensed nebula suggest that star formation is at least powering the Lyα emission from the high surface brightness spots. The enhancement of the blue and/or red peak in these brighter spots either reflects the kinematics of the clumps surrounding these galaxies, where an enhanced blue (red) peak is indicative of clumps falling on to (flowing away from) the galaxies (see Zheng & Miralda-Escudé 2002; Dijkstra, Haiman & Spaans 2006a,b; Verhamme et al. 2006). Alternatively, enhancements in any of the two peaks could be due the galaxies bulk motion with respect to the Lyα emitting nebula (i.e. these could be star-forming galaxies that are moving on to the more massive halo that hosts the Lyα nebula).

Cooling. For massive dark matter haloes ($M_{\mathrm{halo}} \sim 1$–5×10^{12} $M_{\odot}$), the cooling luminosity can reach $L \sim 10^{43}$ erg s^{-1} (e.g. Dijkstra & Loeb 2009; Faucher-Giguère et al. 2010; Goerdt et al. 2010; Rosdahl & Blaizot 2012; Lake et al. 2015), which is sufficient to explain these haloes. The overall double-peaked spectrum is reminiscent of that predicted by Faucher-Giguère et al. (2010) for cooling radiation (though see Trebitsch et al. 2016). In particular, the observed velocity difference (≃650 km s^{-1}) and the Lyα total luminosity are compatible to those reported by Faucher-Giguère et al. (2010). Also in terms of spatial emission, there are similarities, like the extensions of several tens kpc and the emission arising from different places. The spatial extent results from a combination of some of the cooling radiation being emitted in the accretion streams far from the galaxy(ies), and of spatial diffusion owing to resonant scattering. Also the presence of a well-developed blue component slightly broader than the red one is among the outputs of the Faucher-Giguère et al. (2010) prescriptions (see their fig. 5), and is indicative of systematic infall, in which the velocity of the inflowing gas tends to move (in the frequency domain) the red Lyα photons towards the resonance, while making easier for the blue Lyα photons to escape in the blue side.

Fluorescence. It is also possible that ionizing photons escape from galaxies, which would cause the cold clouds to fluoresce in Lyα (e.g. Mas-Ribas & Dijkstra 2016). Fluorescent Lyα emission also gives rise to a double-peaked spectrum, in which infalling/outflowing material diminishes the red/blue wing of the spectrum. However, fluorescence tends to produce a smaller peak separation than what is observed here (e.g. Gould & Weinberg 1996; Cantalupo et al. 2005). In other words, if fluorescence is the source of Lyα emission, then we would still need additional scattering to explain the width of the Lyα line. Note that this explanation also relies on star formation powering the Lyα emission. Given the number of galaxies that are possibly associated with each system, this explanation is energetically compatible with the observed star formation activity (see Rauch et al. 2011). Moreover, as mentioned above, the strong optical rest-frame nebular emission ([O III] λλ4959, 5007 and Hβ) as traced by the *K*-band for some of the galaxies (e.g. no. 3, no. 2, and no. 6 in the *HUDF* nebula and in the lensed nebula) is intriguingly similar to what has been recently observed in a $z = 3.2$ galaxy having equivalent widths of EW([O III] λλ4959, 5007) = 1500 Å (de Barros et al. 2016) and showing a remarkable amount of escaping ionizing radiation (higher than 50 per cent; Vanzella et al. 2016). Among them, it is worth noting the presence of the extremely blue (and in practice dust-free), compact and low-mass

galaxy (no. 6) that might further contribute to the ionization budget. The Lyα resonance emission from nebulae may be indirect probes of the escaping ionizing radiation from the embedded sources (even fainter that the detection limit), along transverse directions not accessible from the observer. While the direct detection of the Lyman continuum emission is in principle possible, it might be precluded in these data because galaxies are surrounded by the same (circumgalactic) medium plausibly producing the Lyα nebula and therefore preventing us from easily detecting ionizing flux. In addition, the intergalactic opacity in the Lyman continuum also affects these measurements (e.g. Vanzella et al. 2012), requiring a larger sample of similar systems to average the IGM stochastic attenuation.

Active galactic nucleus activity. Active galactic nucleus can inject large amount of energy in the surrounding gas (e.g. Debuhr, Quataert & Ma 2012), which could radiate even after the nucleus has shut off. Such processes can modify the kinematic and thermal properties of the circumgalactic medium, and therefore its Lyα signatures.

The key observable that distinguishes between different sources of Lyα emission would be the Balmer emission lines (like Hα or Hβ). In the case of cooling radiation, the Hα flux that is associated with Lyα should be $\sim$ 100 times weaker (Dijkstra 2014), and would likely be undetectable. However, for the 'star formation' and 'fluorescence' models, the Hα flux should be significantly stronger. If Hα emission can be observed, and confined to galaxies, then Lyα emission was likely powered by nebular emission inside galaxies, while fluorescence would give rise to partially extended Hα.

The search for galaxies that illuminate themselves through some fortuitous release of Lyα or ionizing radiation into their environment offers positive prospects in the future MUSE observations and will provide our main direct insights into the inflows and outflows of gas (Rauch et al. 2016). If the scenario in which the gas is inflowing towards a region forming stars is correct, then we may be witnessing an early phase of galaxy or a proto-cluster (or group) formation. Searches for asymmetric Lyα haloes or offsets between stellar populations and Lyα emission may reveal further objects where the escape of ionizing radiation can be studied.

ACKNOWLEDGEMENTS

This paper is based on the observations collected at the European Southern Observatory for Astronomical research in the Southern hemisphere under ESO programmes P096.A-0045 and P094.A-0115. We thank the anonymous referee, F. Calura and G. Zamorani for constructive comments. We gratefully acknowledge M. Rauch for helpful discussions about galaxy no. 10, and A. Grazian for providing us the *K*-band image of the *HUDF* nebula. Part of this work has been funded through the PRIN INAF 2012. We acknowledge financial support from PRIN-INAF 2014, 1.05.01.94.02.

REFERENCES

Adelberger K. L., Steidel C. C., Shapley A. E., Pettini M., 2003, ApJ, 584, 45
Bacon R. et al., 2012, The Messenger, 147, 4
Beckwith S. V. W. et al., 2006, AJ, 132, 1729
Borisova E. et al., 2016, preprint (arXiv:1605.01422)
Caminha G. B. et al., 2015, preprint (arXiv:1512.05655)
Caminha G. B. et al., 2016, preprint (arXiv:1607.03462)
Cantalupo S., Porciani C., Lilly S. J., Miniati F., 2005, ApJ, 628, 61
Cantalupo S., Arrigoni-Battaia F., Prochaska J. X., Hennawi J. F., Madau P., 2014, Nature, 506, 63
Castellano M. et al., 2016, A&A, 590, A31
Chen H.-W., Lanzetta K. M., Webb J. K., Barcons X., 2001, ApJ, 559, 654
Christensen L., Sánchez S. F., Jahnke K., Becker T., Wisotzki L., Kelz A., Popović L. Č., Roth M. M., 2004, A&A, 417, 487
Coe D., Benítez N., Sánchez S. F., Jee M., Bouwens R., Ford H., 2006, AJ, 132, 926
de Barros S. et al., 2016, A&A, 585, A51
Debuhr J., Quataert E., Ma C.-P., 2012, MNRAS, 420, 2221
Dijkstra M., Haiman Z., Spaans M., 2006a, ApJ, 649, 14
Dijkstra M., Haiman Z., Spaans M., 2006b, ApJ, 649, 37
Dijkstra M., Loeb A., 2009, MNRAS, 400, 1109
Dijkstra M., 2014, Publ. Astron. Soc. Aust., 31, e040
Dunlop J. S. et al., 2016, preprint (arXiv:1606.00227)
Elbaz D. et al., 2011, A&A, 533, A119
Faucher-Giguère C.-A., Kereš D., Dijkstra M., Hernquist L., Zaldarriaga M., 2010, ApJ, 725, 633
Fontana A. et al., 2014, A&A, 570, A11
Francis P. J., Dopita M. A., Colbert J. W., Palunas P., Scarlata C., Teplitz H., Williger G. M., Woodgate B. E., 2013, MNRAS, 428, 28
Fynbo J. U., Møller P., Warren S. J., 1999, MNRAS, 305, 849
Fynbo J. P. U., Ledoux C., Møller P., Thomsen B., Burud I., 2003, A&A, 407, 147
Giavalisco M. et al., 2004, ApJ, 600, L93
Giavalisco M. et al., 2011, ApJ, 743, 95
Goerdt T., Dekel A., Sternberg A., Ceverino D., Teyssier R., Primack J. R., 2010, MNRAS, 407, 613
Gould A., Weinberg D. H., 1996, ApJ, 468, 462
Gronke M., Dijkstra M., 2016, ApJ, 826, 14
Guo Y. et al., 2013, ApJS, 207, 24
Hayes M., Scarlata C., Siana B., 2011, Nature, 476, 304
Hennawi J. F., Prochaska J. X., Cantalupo S., Arrigoni-Battaia F., 2015, Science, 348, 779
Harrington J. P., 1973, MNRAS, 162, 43
Lanzetta K. M., Bowen D. V., Tytler D., Webb J. K., 1995, ApJ, 442, 538
Lake E., Zheng Z., Cen R., Sadoun R., Momose R., Ouchi M., 2015, ApJ, 806, 46
Laursen P., Sommer-Larsen J., Razoumov A. O., 2011, ApJ, 728, 52
Lotz J. et al., 2014, Am. Astron. Soc. Meeting Abstr., 223, 254.01
Karman W. et al., 2016, preprint (arXiv:1606.01471)
Koekemoer A. M. et al., 2014, Am. Astron. Soc. Meeting Abstr., 223, 254.02
Kulas K. R., Shapley A. E., Kollmeier J. A., Zheng Z., Steidel C. C., Hainline K. N., 2012, ApJ, 745, 33
Martin D. C., Matuszewski M., Morrissey P., Neill J. D., Moore A., Cantalupo S., Prochaska J. X., Chang D., 2015, Nature, 524, 192
Mas-Ribas L., Dijkstra M., 2016, ApJ, 822, 84
Matsuda Y., Yamada T., Hayashino T., Yamauchi R., Nakamura Y., 2006, ApJ, 640, L123
Miller N. A. et al., 2013, ApJS, 205, 13
Møller P., Warren S. J., 1998, MNRAS, 299, 661
Neufeld D. A., 1990, ApJ, 350, 216
Nonino M. et al., 2009, ApJS, 183, 244
Patrício V. et al., 2016, MNRAS, 456, 4191
Pirzkal N. et al., 2004, ApJS, 154, 501
Prescott M. K. M. et al., 2012, ApJ, 752, 86
Prescott M. K. M., Martin C. L., Dey A., 2015, ApJ, 799, 62
Rafelski M. et al., 2015, AJ, 150, 31
Rauch M., Becker G. D., Haehnelt M. G., Gauthier J.-R., Ravindranath S., Sargent W. L. W., 2011, MNRAS, 418, 1115
Rauch M., Becker G. D., Haehnelt M. G., 2016, MNRAS, 455, 3991
Rosdahl J., Blaizot J., 2012, MNRAS, 423, 344
Santini P. et al., 2009, A&A, 504, 751

Shapley A. E., Steidel C. C., Pettini M., Adelberger K. L., 2003, ApJ, 588, 65
Steidel C. C., Erb D. K., Shapley A. E., Pettini M., Reddy N., Bogosavljević M., Rudie G. C., Rakic O., 2010, ApJ, 717, 289
Swinbank A. M. et al., 2015, MNRAS, 449, 1298
Trebitsch M., Verhamme A., Blaizot J., Rosdahl J., 2016, A&A, 593, A122
Turner M. L., Schaye J., Steidel C. C., Rudie G. C., Strom A. L., 2014, MNRAS, 445, 794
Vanzella E. et al., 2009, ApJ, 695, 1163
Vanzella E. et al., 2012, ApJ, 751, 70
Vanzella E. et al., 2016, ApJ, 825, 41
Verhamme A., Schaerer D., Maselli A., 2006, A&A, 460, 397
Wisotzki L. et al., 2016, A&A, 587, A98
Worseck G. et al., 2014, MNRAS, 445, 1745
Zheng Z., Miralda-Escudé J., 2002, ApJ, 578, 33

This paper has been typeset from a TEX/LATEX file prepared by the author.